TB16

19th International Symposium of Ballistics, 7–11 May 2001, Interlaken, Switzerland

ANALYTICAL MODEL OF LONG ROD INTERACTION WITH SPACED-PLATE TARGETS

S. Chocron[1], C. E. Anderson, Jr.[2], and J. D. Walker[2]

[1] Dpto. Ciencia de Materiales, E.T.S.I. Caminos, Universidad Politécnica de Madrid, Madrid 28040, Spain

[2] Southwest Research lnstitute, P.O. Box 28510, San Antonio, TX 78228-0510, USA

The WAR (Walker-Anderson-Ravid) model was presented at the 17th Int. Symp. on Ballistics, South Africa. The WAR model is based on the Walker-Anderson penetration model for long-rod penetration into semi-infinite targets, combined with various exit or breakout modes that can occur in perforation of finite-thickness targets, as formulated by Ravid and Bodner. This paper presents modifications made to the WAR model to make it applicable to spaced-plate targets. Examples are presented for long-rod projectiles against a thick target backed by a witness pack that is separated by an air gap; and a multiple, spaced-plate target. Agreement with results from numerical simulations is excellent.

INTRODUCTION

The Walker-Anderson [1] and Ravid-Bodner [2] models were “unified” in Ref. [3], obtaining the WAR (Walker-Anderson-Ravid) model, a complete model that accounts for the penetration process and the failure of the target. In the WAR model, a time-dependent penetration model [1] is combined with various exit or breakout modes that can occur in perforation of finite-thickness targets [2]. The combined model [3] was validated with several examples for long-rod projectiles impacting finite-thickness, hard steel targets.

The penetration/perforation mechanics of multiple element targets is quite complex because of target failure; and equilibration, or “relaxation”, of velocity and stress gradients within the projectile prior to impact of the next target element. During penetration of a target, the projectile erodes and decelerates. When the projectile exits, i.e., perforates, the target, the projectile continues to erode due to residual stresses within the nose area of the rod. Also, rarefaction waves travel along the projectile until it is moving at a uniform residual velocity. These two physical effects must be taken into account to model analytically multiple-plate target interactions. This paper presents modifications made to the WAR model to make it applicable to spaced-plate targets.

Two multiple element target examples are presented, with each example having two long-rod projectiles impacting at different velocities. All the examples presented in this paper are taken from Ref. [4]; additional details on the experimental results are provided in Ref. [5]. The projectiles had a length-to-diameter (LID) ratio of 30, and were equal kinetic energy projectiles. Information on the projectiles is summarized in Table 1. The targets are described later.

Table 1: Projectile Geometry

	Projectile 1	Projectile 2
Impact Velocity (km/s)	1.775	2.60
Mass (g)	1830	850
Length (cm)	49.4	38.4
Diameter (cm)	1.65	1.28

THE MODEL

When the target "fails", that is, there is "perforation", the projectile no longer encounters any further resistance but projectile erosion continues some microseconds because of the large residual stresses in the plastic zone. Reference [4], studies the history of the projectile length, as calculated using numerical simulations, for tungsten-alloy projectiles penetrating a 45.7-cm-thick RHA target. Behind the RHA target, separated by an air gap of 7.62 cm, is a RHA witness pack. Between exit from the rear surface of the target and the beginning of penetration into the witness pack, the projectile length decreases (erodes) by approximately one projectile diameter. This effect is not particularly large (nominally one part in 30) for single-plate targets, but the cumulative effect for multiple-plate targets would result in substantial errors and thus cannot be ignored.

Relaxation Time

We are interested in cases where penetration stresses are sufficiently high that the projectile material is plastically deforming and eroding. The plastic extent in the projectile can be calculated with the equation found in Ref. [1]:

$$s = \frac{R}{2}\left(\frac{v}{u} - 1\right)\left(1 - \frac{1}{\alpha^2}\right) \tag{1}$$

where s is the plastic extent in the projectile, R the crater radius, v the velocity of the tail of the projectile, u the velocity of the tip, and α is the extent of plastic flow (normalized by the crater radius) in the target.

Using results from numerical simulations, it is possible to estimate the length of time it takes for the projectile to equilibrate in velocity. Elastic waves traveling within the projectile are responsible for velocity equilibration, so one possibility to estimate this relaxation time is assume that it is proportional to the time it takes for an elastic wave to go and

come back from nose to tail. But the results shown in Fig. 1 suggest that the relaxation time does not depend on projectile length. The plot shows the velocity of nose and tail of a long-rod tungsten-alloy projectile impacting a spaced target (6 plates). As the nose perforates a plate, the nose velocity increases, trying to equilibrate with the tail velocity. (Most of the projectile material has the speed of the tail [5], and therefore, the tail velocity – until the projectile becomes relatively short – dominates in determination of the equilibration velocity [6].) The time taken to relax between two consecutive plates does not depend on which plate is being penetrated. Consequently, since the projectile is shorter after each of the impacts, the relaxation time does not appear to depend strongly on the length of the projectile. More likely, the relaxation time depends on the size of the plastic zone in the projectile, and the plastic zone is proportional to the projectile radius (since the crater radius R is proportional to the projectile radins R_p).

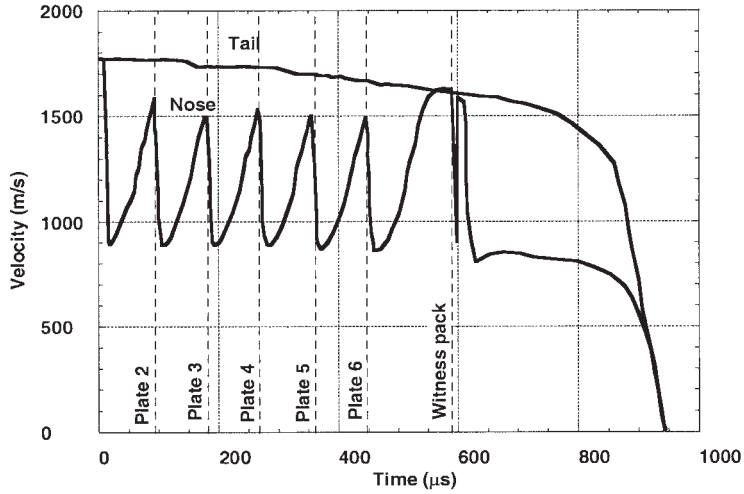

Figure 1: Simulation results for nose and tail velocities of a tungsten-alloy projectile impacting 6 spaced plates.

In this paper the time assumed for relaxation is given by:

$$t_{relax} = 30\frac{R_p}{c_p} \tag{2}$$

where R_p is the radius of the projectile and c_p the sound speed of the projectile material.

Velocity of the projectile after relaxation

Between failure of a plate and relaxation of projectile no force is acting on the projectile. The total momentum is then constant allowing the calculation of the velocity after relaxation. When the plate fails the velocity profile in the projectile is constant (say V_{fail}) from the tail to the rear of the plastic zone, and then decreases linearly in the plastic zone to the penetration velocity u_{fail}, see Refs. [1,6] for more details. Assuming that the length

of the projectile just before failure be L_{fail}; the plastic extent s_{fail}; the tail and nose velocities are V_{fail} and u_{fail}, respectively; then the velocity V_{relax} of the (now rigid) projectile after equilibration (relaxation) is given by:

$$V_{relax} = \frac{(L_{fail} - s_{fail})}{L_{fail}} V_{fail} + \frac{s_{fail}}{L_{fail}} \left(\frac{V_{fail} + u_{fail}}{2} \right) \tag{3}$$

The projectile might impact the next target element before achieving total equilibration, as for example is shown in Fig. 2. Therefore Eq. (3) does not provide sufficient information, and an expression for the "nose velocity" u is needed for the free flight.

Velocity of the nose and tail during free flight

The velocity of the nose during the free flight is assumed to increase linearly with time from its velocity at the instant of failure, u_{fail}, to its equilibration velocity, V_{rel}:

$$u(t) = u_{fail} + \left(\frac{V_{relax} - u_{fail}}{t_{relax} - t_{fail}} \right) (t - t_{fail}) \tag{4}$$

The same assumption gives the velocity of the tail:

$$v(t) = v_{fail} + \left(\frac{V_{relax} - v_{fail}}{t_{relax} - t_{fail}} \right) (t - t_{fail}) \tag{5}$$

Equations (4) and (5) are valid only when $t < t_{relax}$. The position of the nose at any time as well as at the instant of the impact with the next target element are easily calculated with the integration of Eq. (4). The difference between Eqs. (4) and (5) gives the erosion rate (a negative quantity since the projectile is shortening); and integration of the erosion rate over time provides the decrease in projectile length.

Equations (2) to (4), together with the WAR model found in Ref. [3], allow the solution o long rod projectiles impacting semi-infinite or finite spaced targets. The residual velocity and residual length from perforation of one target element are used as the "initial" conditions for impact with the next target element.

EXAMPLE 1: LONG ROD AGAINST RHA TARGET AND WITNESS PACK

All the examples presented in this paper are taken from Ref. [4]. The first example is the impact of a tungsten-alloy, long-rod projectile penetrating a 45.72-cm-thick RHA target. Behind the target, separated by a 7.62-cm air gap, is a RHA witness pack. Tables 1 and 2 list the geometry and material properties used for the calculations. Figure 2 shows both the numerical and analytical position vs. time plots for the two projectiles. The numerical simulations results, from the Eulerian wavecode CTH, are shown as circles. The CTH results matched the experimental depths of penetration into the witness pack, so the analytical model is compared to the time history numerical results. The predictions of the model are in excellent agreement with the numerical simulations.

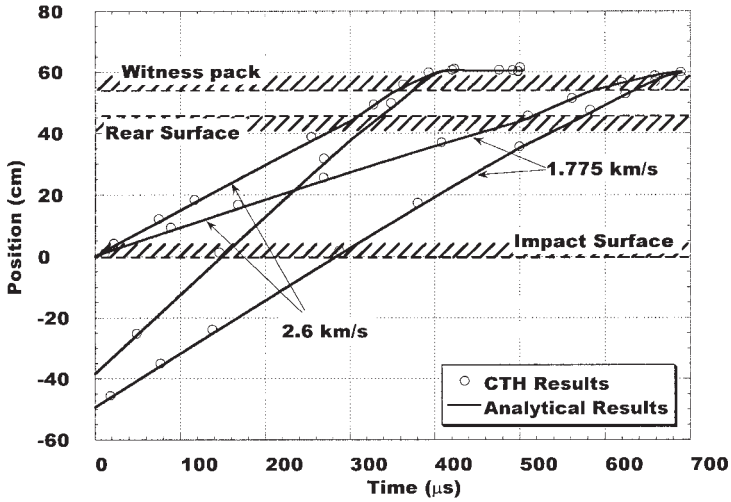

Figure 2: Positions of tail and nose of the projectile calculated numerically (CTH) and analytically.

Figure 3 depicts the history of velocities of the tail and nose for the two projectiles considered. It is pointed out that the peaks of the nose velocity happen when the projectile is in free flight. In this example the air gap of 7.62 cm is sufficiently wide to allow for the projectile velocity to equilibrate (relax) completely before impacting the witness plate. The agreement between the model and the numerical simulations is again very good during penetration of the RHA target and during the free flight. The agreement is not quite so good in the penetration of the witness pack because the projectile, by this time, has a 1ow aspect ratio, and the assumption that the tail portion of the projectile is in a state of uniaxial stress is no longer valid. Nevertheless, overall agreement is quite good.

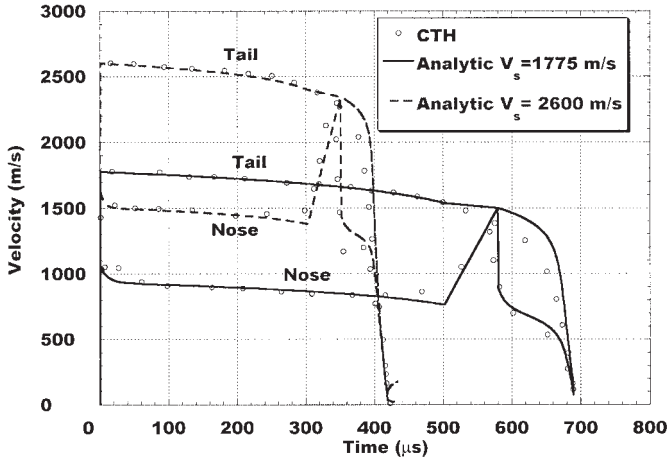

Figure 3: Time histories of the tail and nose velocities for numerical (CTH) and analytical model results.

EXAMPLE 2: LONG ROD AGAINST 6 SPACED PLATES & WITNESS PACK

In this example, the long rods (same as in the first example) were fired against 6 high-hard steel plates, each 1.90-cm thick, inclined at 65° (NATO angle), and separated by air gaps of 2.54 cm. The witness pack was placed 7.62 cm behind the last plate. To account for target obliquity in the analytical model, it was assumed that the effective plate thicknesses should be the line-of-sight thicknesses as seen by the projectile. Therefore, the target elements were increased by 1/cos 65°.

Table 2: Material properties used in the analytical calculations

Projectile density (g/cm^3)	17.4	Target yield strength (GPa)	1.2
Projectile yield strength (GPa)	1.5	Target shear modulus (GPa)	77.7
Speed of sound in the projectile (km/s)	3.85	Target sound velocity (km/s)	4.50
Slope of Hugoniot (tungsten, n.d.)	1.44	Slope of Hugoniot (steel, n.d.)	1.49
Target density (g/cm^3)	7.85	Strain to failure in target (n.d.)	0.65

It is more difficult to assess the accuracy for this example. The numerical simulations overpredicted the depth of penetration into the witness pack, at each of the impact velocities, by approximately 4 cm. Most likely, this is due to an inadequate treatment of failure at the projectile nose and/or breakout (failure) from each of the target elements. Unfortunately, however, the depth of penetration into the witness pack is essentially the only diagnostic from the experiment. Numerical simulations provide time histories of penetration, which allow for better comparisons, so comparisons are made with the simulation results.

Position versus time for the fast and slow projectiles from the simulations and the analytical model are compared in Fig. 4; again, the circles represent the simulations results, and the lines the results from the analytical model. Agreement is very good for the 2.60-km/s projectile. For the lower velocity projectile the analytical model underpredicts the depth of penetration into the witness pack, but is in better agreement with the experimental results.

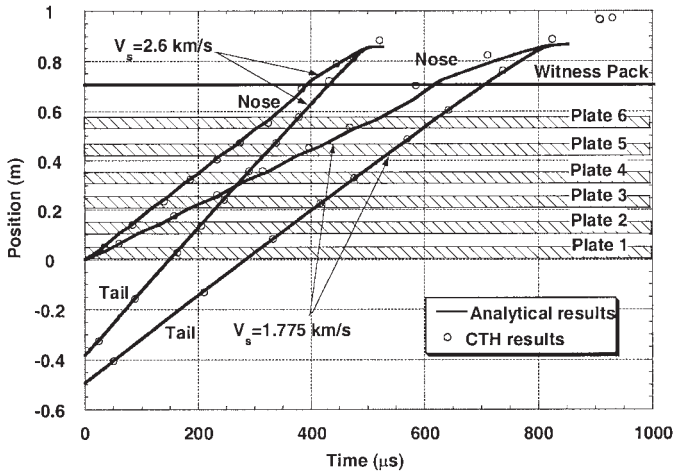

Figure 4: Position-time histories for numerical (CTH) and analytical models for the 6-plate impact example.

The time histories of the nose and tail of the projectiles are plotted in Fig. 5. Predictions of the analytical model are in very good agreement for the hypervelocity projectile. For the 1.775-km/s projectile, a shift between the analytical and numerical calculations is observed in the impact timing. The cause for this shift is that the numerical calculation is 3-D, allowing for the formation of an asymmetric mushroom head on the nose of the projectile. (An asymmetric mushroom nose also forms on the 2.60-km/s projectile, but the diameter of this projectile is smaller, and therefore, the effect is less pronounced. Further, the velocity is higher, so strength effects are not as significant as at the lower velocity.) Because of the obliquity of the target plates, the "side" of the mushroom impacts the plates and interaction starts sooner than for normal impact. Multiple applications of this affect results in a cumulative shift in the time. The analytical model does not predict as deep penetration as the numerical simulations, as already discussed, so the total time of penetration is correspondingly less.

CONCLUSIONS

The Walker-Anderson-Ravid model has been modified to allow calculations of multiple element targets. The phenomena of multiple plate penetration, target obliquity, target failure, and velocity and stress relaxation of the projectile after perforation result in very complex mechanics. Even with this complexity, the modified model is able to reproduce most of the physics sufficiently accurately to provide fairly good agreement with numerical simulations (which, as pointed out, have their own inaccuracies) and experimental results. It is suggested that the model be validated against additional multiple plate impact experiments, which the authors hope to do in the near future.

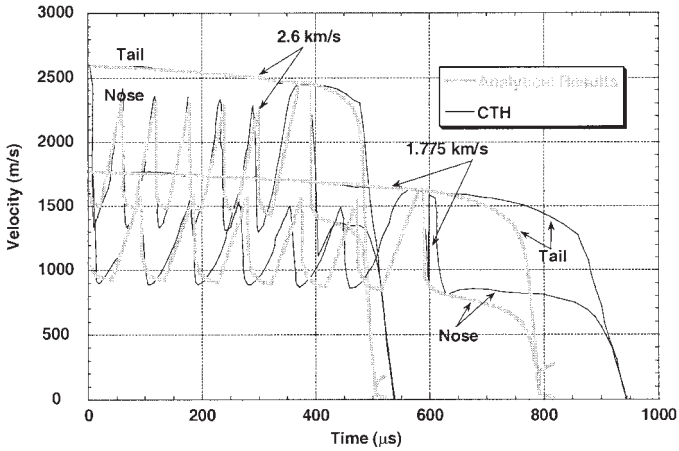

Figure 5: Time histories of the tail and nose velocities for numerical (CTH) and analytical model for the 6-plate impact example.

REFERENCES

1. J. D. Walker and C. E. Anderson, Jr., "A Time-Dependent Model for Long-Rod Penetration," *Int. J. Impact Engng.*, **16**(1), 19–48, 1995.
2. M. Ravid and S. R. Bodner, "Dynamic Perforation of Viscoplastic Plates by Rigid Projectiles," *Int. J. Engng. Sci.*, **21**(6), 577–591, 1983
3. M. Ravid, S. R. Bodner, J. D. Walker, S. Chocron, C. E. Anderson, Jr., J. P. Riegel, III, "Modification of the Walker-Anderson Model to Include Exit Failure Modes and Fragmentation," *17th Int. Symp. on Ballistics*, Vol. 3, pp. 267–274, Midrand, South Africa, March 23–27, 1998.
4. C. E. Anderson, Jr. and D. L. Littlefield, "Pretest Predictions of Long-Rod Interactions with Armor Technology Targets," SwRI Report 07-5117, prepared for the U. S. Army Research Office, Southwest Research Institute, San Antonio, TX, April 1994.
5. C. E. Anderson, Jr., S. J. Bless, D. L. Littlefield, and R. Subramanian, "Prediction of Large Scale Impact Experiments on Steel Targets," *14th Int. Symp. on Ballistics*, Vol. 2, pp. 459–468, Quebec, Canada, Sept. 26–29, 1993.
6. C. E. Anderson, Jr. and J. D. Walker, "An Examination of Long-Rod Penetration," *Int. J. Impact Engng.*, Vol. 11, No. 4, pp. 481–501, 1991.
7. C. E. Anderson, Jr., V. Hohler, J. D. Walker, and A. J. Stilp, "The Influence of Projectile Hardness on Ballistic Performance," *Int. J. Impact Engn.*, **22**(6), 619–632, 1999.